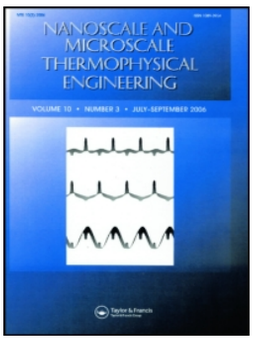

Nanoscale and Microscale Thermophysical Engineering

ISSN: 1556-7265 (Print) 1556-7273 (Online) Journal homepage: http://www.tandfonline.com/loi/umte20

High Power Density Pyroelectric Energy Conversion in Nanometer-Thick $BaTiO_3$ Films

Bikram Bhatia, Hanna Cho, J. Karthik, Jangho Choi, David G. Cahill, Lane W. Martin & William P. King

To cite this article: Bikram Bhatia, Hanna Cho, J. Karthik, Jangho Choi, David G. Cahill, Lane W. Martin & William P. King (2016) High Power Density Pyroelectric Energy Conversion in Nanometer-Thick $BaTiO_3$ Films, Nanoscale and Microscale Thermophysical Engineering, 20:3-4, 137-146, DOI: 10.1080/15567265.2016.1252820

To link to this article: http://dx.doi.org/10.1080/15567265.2016.1252820

NANOSCALE AND MICROSCALE THERMOPHYSICAL ENGINEERING
2016, VOL. 20, NOS. 3–4, 137–146
http://dx.doi.org/10.1080/15567265.2016.1252820

Taylor & Francis
Taylor & Francis Group

High Power Density Pyroelectric Energy Conversion in Nanometer-Thick $BaTiO_3$ Films

Bikram Bhatia[a], Hanna Cho[a], J. Karthik[b], Jangho Choi[a], David G. Cahill[b], Lane W. Martin[c], and William P. King[d]

[a]Department of Mechanical Science and Engineering, University of Illinois Urbana–Champaign, Urbana, Illinois, USA; [b]Department of Materials Science and Engineering and Materials Research Laboratory, University of Illinois Urbana–Champaign, Urbana, Illinois, USA; [c]Department of Materials Science and Engineering and Materials Research Laboratory, University of Illinois Urbana–Champaign, Urbana, Illinois, USA, and Department of Materials Science and Engineering, University of California, Berkeley, California, USA; [d]Department of Mechanical Science and Engineering, University of Illinois Urbana–Champaign, Urbana, Illinois, USA, and Department of Materials Science and Engineering and Materials Research Laboratory, University of Illinois Urbana–Champaign, Urbana, Illinois, USA

ABSTRACT

Solid-state pyroelectric nanomaterials can be used for thermal-to-electrical energy conversion in the presence of temperature fluctuations. This article reports investigation of energy conversion in a 200 nm thick $BaTiO_3$ film using the pyroelectric Ericsson cycle at cycle frequencies up to 3 kHz. The high cycle frequencies were achieved due to the low thermal mass of the nanometer-scale film, unlike previous studies in which the electrical power output was limited by the rate of heat transfer through the pyroelectric material. A micro-fabricated platform that allowed precise thermal and electrical cycling enabled us to study the effect of electric field range, temperature oscillation amplitude, and cycle frequency on the electrical power output from pyroelectric Ericsson cycles. We measured a maximum power density of 30 W/cm^3 for a temperature range 20–120°C and electric field range 100–125 kV/cm, which represents a significant improvement over past work on pyroelectric cycles. The approach presented in this article could lead to high-power waste heat harvesting in systems with high-frequency temperature oscillations.

ARTICLE HISTORY
Received 11 September 2016

KEYWORDS
Pyroelectric energy conversion; waste heat harvesting; pyroelectric Ericsson cycle; thin films

Introduction

Direct conversion of temperature fluctuations to electrical energy using pyroelectric materials has been widely studied for harvesting waste heat [1, 2]. However, direct conversion of this kind is inefficient, and modern approaches to pyroelectric energy conversion rely on thermodynamic cycles that simultaneously vary the temperature and electric fields to enhance the efficiency and allow for continuous operation. Such approaches have been widely reported in the literature [3–6]. In particular, energy conversion using thermal–electrical cycles such as the pyroelectric Ericsson cycle have been shown to give 100 times higher energy output in comparison to direct pyroelectric effect, which utilizes only thermal cycles [5].

A pyroelectric energy conversion cycle generates electrical work from the temperature (T) and electric field (E) driven changes in the electric displacement (D) of the pyroelectric material. The first theoretical studies of pyroelectric energy conversion claimed that pyroelectric energy conversion has unacceptably poor performance, with maximum possible energy conversion efficiency below 1% [7, 8]. Subsequent experiments showed that thermal–electrical cycles can achieve power density of 0.11 W/cm^3, energy

CONTACT William P. King wpk@illinois.edu Department of Mechanical Science and Engineering, University of Illinois Urbana–Champaign, 1206 West Green St., MEL 4409, Urbana, Illinois, 61801.

Color versions of one or more figures in the article can be found online at www.tandfonline.com/umte.

density of 1 J/cm^3, and efficiency of ~5% of the Carnot limit [9–11]. The key to this improved performance was the utilization of thermal–electrical cycles operating close to the ferroelectric phase transition at high electric fields. Previous publications have focused on pyroelectric energy conversion cycles in bulk samples [4, 5, 10, 12, 13] and thick polymer films [14–16], with thermal cycling rates typically slower than 1 Hz [6, 9, 12]. Thin films offer an opportunity for microsystems integration and rapid switching that could lead to high-power-density thermal-to-electrical energy conversion using high-frequency pyroelectric cycles. However, very few studies have investigated pyroelectric energy conversion using thermal–electrical cycles in micrometer- and nanometer-thick films (see supplemental material for a summary of past work). This article investigates high-frequency thermal-to-electrical energy conversion in a 200 nm thick $BaTiO_3$ film using the pyroelectric Ericsson cycle.

Figure 1 shows the pyroelectric Ericsson cycle consisting of two isothermal and two isoelectric processes [4, 5]. The cycle is completed by first applying an electric field aligned with the polar axis of the $BaTiO_3$ film such that the electrical displacement is increased at a constant temperature (A–B). Next, the temperature is increased at constant electric field (B–C), thereby decreasing the electric displacement. From here the electric field is decreased (C–D), again lowering the electric displacement. Finally, the film is cooled back to the starting temperature and recovers the initial electric displacement (D–A). Each displacement change results in a current in the external circuit. The net electric work includes the pyroelectric contribution $\left(E_{BC}\int_{T_B}^{T_C} p_{BC}dT + E_{DA}\int_{T_D}^{T_A} p_{DA}dT\right)$ and the dielectric contribution $\left(\int_{E_A}^{E_B} \varepsilon_{AB}EdE + \int_{E_C}^{E_D} \varepsilon_{CD}EdE\right)$, where $p = \left(\frac{dD}{dT}\right)_E$ is the pyroelectric coefficient and $\varepsilon = \left(\frac{dD}{dE}\right)_T$ is the dielectric permittivity [17]. The heat input includes the energy required to change the electric displacement $\left(T_{AB}\int_{T_A}^{T_B} p_{AB}dE + T_{CD}\int_{T_C}^{T_D} p_{CD}dE\right)$ and that required to heat the lattice $\left(\int_{T_B}^{T_C} c_{BC}dT + \int_{T_D}^{T_A} c_{DA}dT\right)$, where $c = \left(\frac{dU}{dT}\right)_E$ is the heat capacity and U is the internal energy. The thermodynamic efficiency is the net

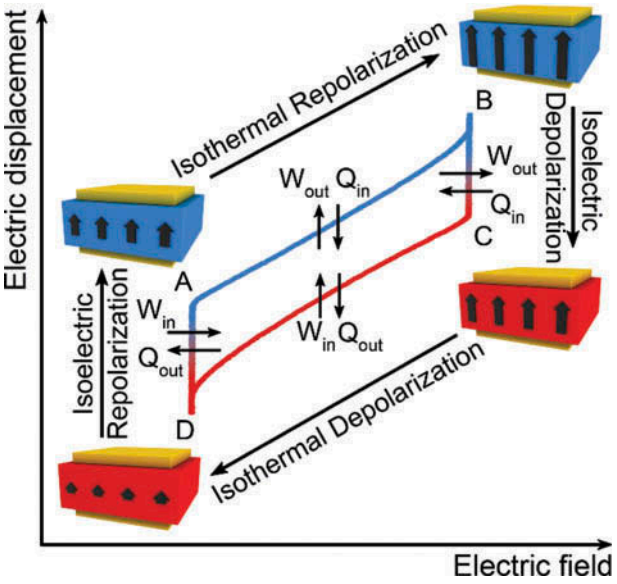

Figure 1. Illustration of the pyroelectric Ericsson cycle on an electric displacement versus electric field plot. The thermodynamic cycle consists of four steps. A → B: Increase in electric field at low temperature; B → C: increase in temperature at high electric field; C → D: decrease in electric field at high temperature; and D → A: decrease in temperature at low electric field.

work out divided by the heat in and is limited by the large irreversible lattice heat contribution [3]. A previously published study investigated the effect of electric field and temperature change rates on the output energy density of thermal–electrical cycles [18]. This work focuses on the electrical power density output from a pyroelectric Ericsson cycle operating on a $BaTiO_3$ thin film and its dependence on the electric field range, temperature oscillation amplitude, and cycle frequency.

Experimental methods

A microfabricated device capable of precise thermal cycling and electric switching and low thermal mass of the thin film enables fast cycle rates, which can in turn lead to high power generation. Figure 2 shows a schematic of the microfabricated platform that allows rapid switching of the temperature and electric fields. The device consists of a 200 nm thick $BaTiO_3$ thin-film capacitor with epitaxial top and bottom $SrRuO_3$ electrodes ($500 \times 20\ \mu m^2$ area), fabricated via pulsed-laser deposition on a $GdScO_3$ (110) single-crystal substrate. A blanket layer of SiO_2 covers the $SrRuO_3/BaTiO_3/SrRuO_3$ heterostructure with openings to access the top and bottom $SrRuO_3$ electrodes. A 15 μm wide platinum strip sits atop the electrically insulating SiO_2 layer and serves as the heater. Additional details of the device fabrication are reported elsewhere [18].

We characterized the physical and electrical properties of the pyroelectric film using an $SrRuO_3/BaTiO_3/SrRuO_3$ sample similar to the device shown in Figure 2 but with blanket $BaTiO_3$ and bottom electrode layers. X-ray diffraction of the as-grown films indicate single-phase (00*l*) oriented films (Figure 3a). Figure 3b shows the atomic force microscope topography of the deposited $BaTiO_3$ film before the top $SrRuO_3$ electrode deposition. The root mean square roughness of the film was 1.1 nm. Figure 3c shows the hysteresis loops for the $BaTiO_3$ capacitor. The temperature-dependent dielectric constant and resistivity of the $BaTiO_3$ film were measured using a sinusoidal excitation voltage of 0.1 V_{RMS} at 100 Hz. At room temperature, the dielectric constant was measured to be 800, and the resistivity was measured to be 10^8 Ω-cm. The dielectric constant maxima corresponding to the Curie temperature (T_C) of the $BaTiO_3$ film lies is in the range 120–150°C, which is consistent with reported literature values for bulk $BaTiO_3$ [19].

The pyroelectric Ericsson cycle was experimentally realized by controlling the time-dependent temperature and external electric field across the $BaTiO_3$ film (Figure 4). A periodic voltage applied to the platinum heater causes resistive heating, which results in a periodic temperature oscillation. The amplitude of temperature oscillations was calculated as a function of frequency from the solution of the heat diffusion equation [18, 20]. A periodic electric field, phase-synced with the heating, applied across the film thickness completes the cycle.

We operated the Ericsson cycle with different electric fields, temperatures, and frequencies. The low temperature for all cycles was maintained at 20°C. The temperature oscillation amplitude at a particular heating frequency was varied between 50 and 100°C by varying the input sinusoidal

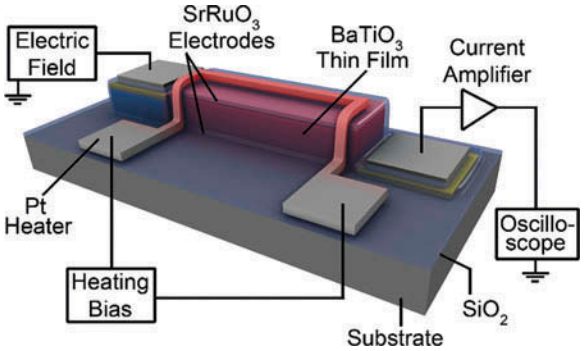

Figure 2. Schematic of the microfabricated device and setup used to implement the pyroelectric Ericsson cycle on a 200 nm thick $BaTiO_3$ film.

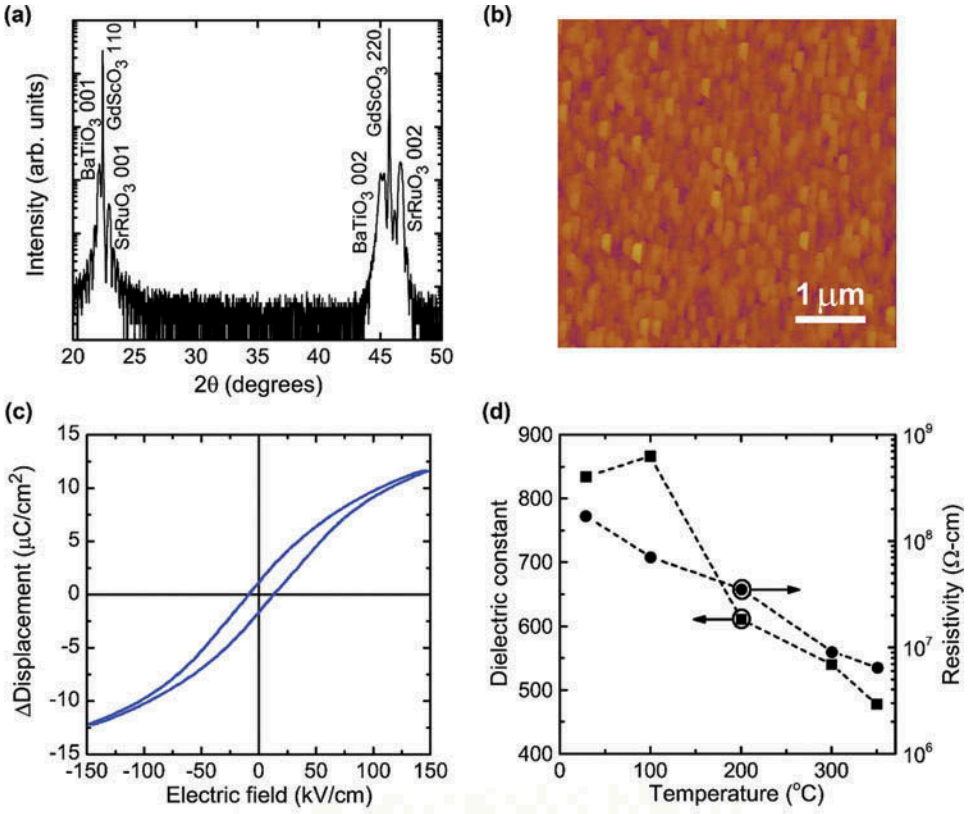

Figure 3. (a) X-ray diffraction pattern of a 150 nm thick $BaTiO_3$ film on $SrRuO_3/GdScO_3$. (b) 5 μm × 5 μm atomic force microscope height image of the $BaTiO_3$ film. (c) *D-E* loops measured using a triangular waveform at 2 kHz. (d) Film dielectric constant and resistivity as a function of sample temperature.

heating voltage across the platinum strip. A step voltage, phase-synced with the heating bias, was applied to the top $SrRuO_3$ electrode. The Ericsson cycle upper voltage across the 200 nm film was maintained at 2.5 V and the lower voltage was varied from 2.25 to 1.25 V. The voltage across the film thickness was switched between the high and low limits at the estimated temperature extrema. The slew rate for the voltage step at 1-kHz cycle frequency was 6.85 kV/s. The film electric displacement changes in response to variations in temperature (pyroelectric contribution) as well as electric field (dielectric contribution) and was calculated by numerical integration of the ac current measured from the bottom $SrRuO_3$ electrode using a current-to-voltage converter. The heating bias, external voltage across the film thickness, and current from the bottom electrode were acquired using an oscilloscope with >16,000 samples per cycle, such that the measurements capture the cycle performance with very high temporal resolution.

Results and discussion

Figure 5 shows the measured Ericsson cycle between 20 and 100°C at a 1 kHz cycle frequency and the corresponding isothermal ferroelectric hysteresis loops. The areas of the shown electric displacement-applied electric field loops represent the electrical energy density. The ferroelectric hysteresis loops progress in a counterclockwise fashion, which represents electricity dissipation as heat [21]. The Ericsson cycle, however, progresses in a clockwise fashion and represents electricity generation from heat. The mismatch between the measured ferroelectric hysteresis loops and Ericsson cycle is due

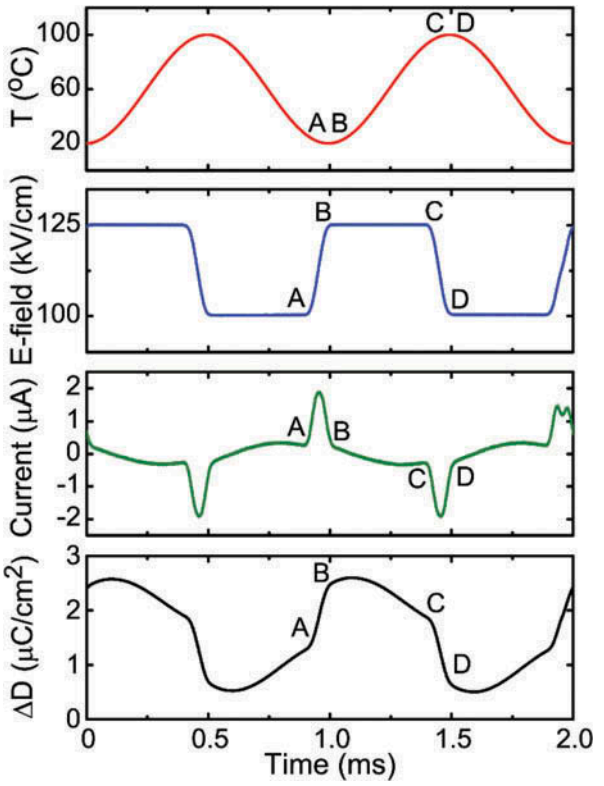

Figure 4. $BaTiO_3$ film temperature, applied electric field, resulting current, and electric displacement change versus time.

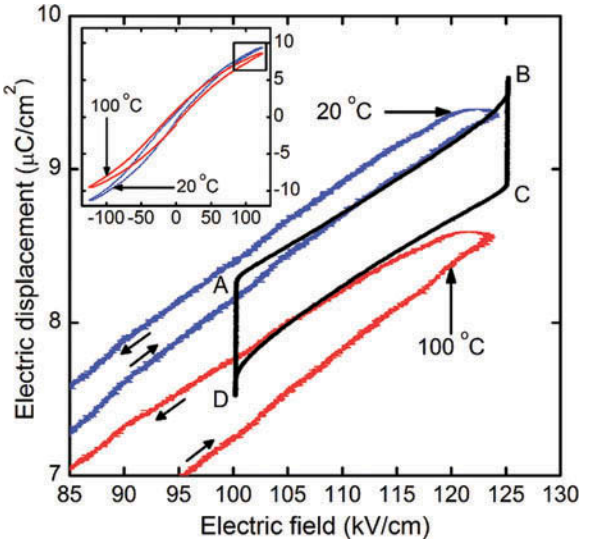

Figure 5. Measured Ericsson cycle shown on a *D-E* plot alongside hysteresis loops (inset) at low and high temperatures.

to the phase difference between the calculated temperature profile and the applied electric field [18]. The spikes at states B and D in the *D-E* diagram are likely due to a small mismatch between the timing of the peak temperature of the pyroelectric film and the electric field switch. Because the pyroelectric film is

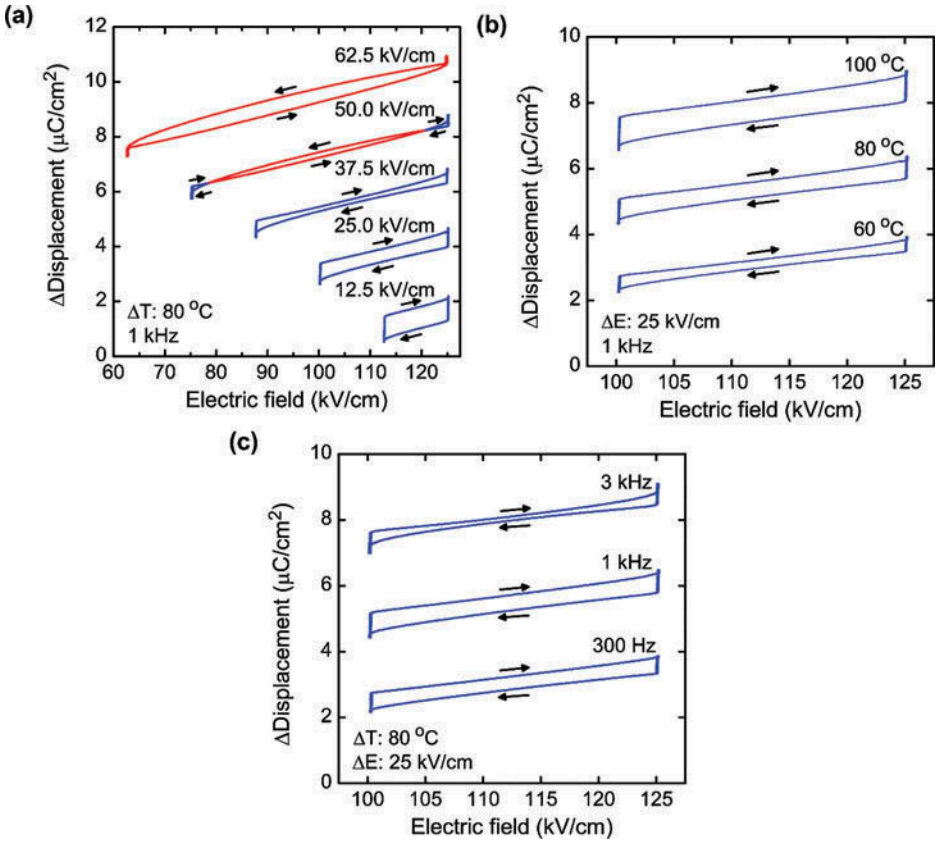

Figure 6. Pyroelectric Ericsson cycles are shown for different (a) ΔE, (b) ΔT, and (c) cycle frequencies. The clockwise cycles shown in blue represent energy generation and the counterclockwise cycles shown in red represent energy dissipation. A maximum electric field of 125 kV/cm and low temperature of 20°C was used for all cycles.

physically separated from the platinum heater strip and since we perform these measurements at millisecond timescales, we believe that the pyroelectric film temperature lags behind the heater strip temperature. Indeed, the spikes vary based on the slew rate at which the electric field switches between its high and low values [18], consistent with the timescale of heat diffusion between the heat source and the pyroelectric film.

The electrical work output from the pyroelectric Ericsson cycle realized in our device varies with the range of applied electric field (ΔE), temperature oscillation amplitude (ΔT), and cycle frequency. Figure 6a shows Ericsson cycles with a maximum electric field of 125 kV/cm and different minimum electric fields. Larger values of ΔE generate counterclockwise cycles that correspond to net work in (heat dissipation), whereas smaller values of ΔE generate clockwise cycles that correspond to net work out (electricity generation). The overall work out depends upon the competition between the pyroelectric contribution and the counteracting dielectric loss originating from the temperature dependence of dielectric permittivity between 20 and 100°C (Figure 3) [17]. In our system, the relatively large dielectric loss is due to the large applied electric fields applied across the thin film and relatively small pyroelectric coefficient of the $BaTiO_3$ layer [18]. The net electrical work out also depends upon ΔT (Figure 6b) and cycle frequency (Figure 6c). Increasing the ΔT while maintaining the same ΔE and fixing the low temperature at 20°C results in an increase in electric displacement change due to the pyroelectric effect. However, changing the cycle frequency for a given ΔE and ΔT results in no significant change in the pyroelectric and dielectric response of the material [22].

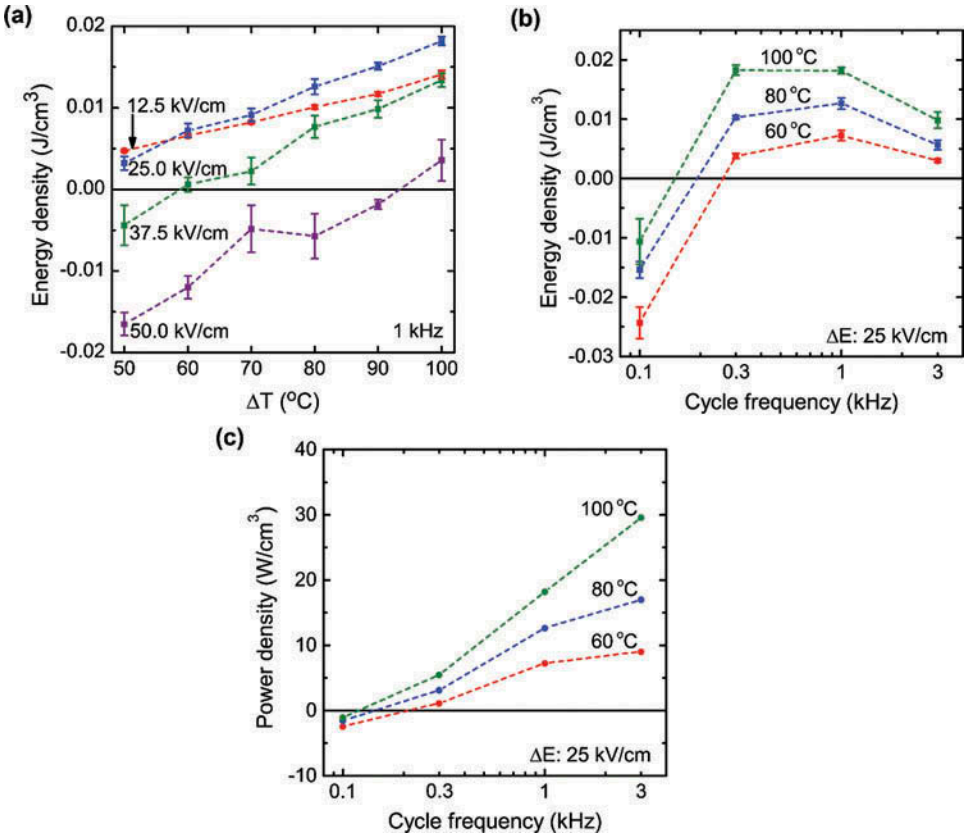

Figure 7. (a) Measured energy density as a function of ΔT for different electric field ranges. Measured (b) energy density and (c) power density as a function of cycle frequency for different ΔT. A maximum electric field of 125 kV/cm and low temperature of 20°C was used for all cycles. The error bars for energy density were obtained using data from four cycles.

The energy density and power density of the pyroelectric Ericsson cycle depend upon the operating conditions. Figure 7a shows the measured energy density as a function of ΔT, which depends upon ΔE as discussed above. Figure 7b shows the measured energy density as a function of the cycle frequency. The error bars represent the standard deviation in the measured energy density due to experimental variations such as contact resistance between probes and device electrodes as well as minor fluctuations in the polarization of the ferroelectric film between multiple cycles. The Ericsson cycle energy density does not change significantly with cycle frequency because the pyroelectric and dielectric responses of the $BaTiO_3$ film are nearly constant in the frequency range investigated [1, 22]. The measured energy density is about the same for 300 Hz and 1 kHz; however, it decreases for the highest and lowest frequencies. At 100 Hz, the negative energy density is likely due to electrical losses in the pyroelectric film (see supplemental material). At 3 kHz, reduction in the measured energy density is due to operation faster than the device thermal time constant. The thermal penetration depth is larger than the $BaTiO_3$ film thickness, resulting in a near-uniform temperature field in the device for all but the highest operating frequencies (see supplemental material) [23]. Figure 7c shows the power density as a function of cycle frequency, calculated by multiplying the energy density per cycle with the number of cycles per unit time. The power density is directly proportional to the cycle frequency until 3 kHz, which is a limit set by our particular device design.

A maximum power density of 30 W/cm^3 was measured at 3 kHz cycle frequency for a temperature range of 20–120°C and an electric field range of 100–125 kV/cm. This power density is significantly

greater than the maximum previously reported for pyroelectric cycles of 0.11 W/cm^3 [9]. However, the corresponding energy density was only ~0.01 J/cm^3 and the efficiency was ~0.03% of Carnot. This energy density is less than the maximum reported values at low cycle frequencies [10]. The low energy density and conversion efficiency were due to the relatively low pyroelectric coefficient of the $BaTiO_3$ film and large dielectric losses [18]. The finite resistivity of the $BaTiO_3$ film (Figure 3d) also contributed to the electrical loss via leakage currents [24]. Though the leakage current limited the net electricity generation, Joule heating in the film was negligible relative to the heat input.

By shrinking our pyroelectric material to the nanometer scale, we were able to study the effect of electric field range and temperature oscillation amplitude on the electrical power density output from Ericsson cycles at high cycle frequencies. This is in contrast to the published literature on pyroelectric energy conversion, where energy conversion in thick films and bulk samples is limited by heat transfer in the pyroelectric material [4, 5, 12–16]. In our setup, the pyroelectric energy conversion was limited by dielectric losses due to the high electric fields in the thin films and relatively low pyroelectric coefficient of the proof-of-concept material system chosen for this study.

Significant improvement in energy and power densities is possible by using films with high pyroelectric coefficients and engineering materials with less electrical losses. Recent studies have reported energy densities up to 0.9 J/cm^3 from Olsen cycles operating on micrometer-thick films of lead lanthanum zirconate titanate and poly(vinylidene fluoride-trifluoroethylene) at cycle frequencies less than 0.1 Hz [15, 16, 25]. The large energy densities were primarily a result of the high intrinsic pyroelectric coefficients of the chosen material systems. Even higher energy densities were achieved by exploiting the ergodic relaxor–ferroelectric phase transition in lead lanthanum zirconate titanate samples [10]. Though further optimization is possible by matching the ferroelectric–paraelectric phase transition temperature with a particular heat source, the change in power output due to operation near the transition temperature may not be significant due to the broad second-order phase transition characteristic of ferroelectric thin films [26]. Additional improvements in the electrical energy output can be achieved by minimizing the dielectric and resistive losses; for example, by increasing the film resistance via cation co-doping [27, 28].

In addition to the materials challenges, several aspects related to the practical implementation of pyroelectric cycles for energy harvesting and integration of thin-film energy harvesters in real devices need to be addressed. Though energy and power densities can be large for thin films, the total energy and power are limited due to the small material volume. Furthermore, the operation of thermal–electrical cycles such as the Ericsson cycle require temporal control of the electric field across the pyroelectric film in synchrony with the temperature oscillations. Previous studies have proposed using electronic switches between the active material and an energy storage cell to control the electrical charge across the pyroelectric capacitor [29]. However, the non-zero leakage currents of switches and energy storage cells limit the overall efficiency and need further development.

Conclusion

We have investigated pyroelectric energy conversion in a 200 nm thick $BaTiO_3$ film using a microfabricated platform that allows synchronous thermal and electrical cycles. We were able to study pyroelectric energy conversion cycles in the 100 Hz–3 kHz frequency range, in contrast to previous studies that operated typically at less than 1 Hz. The high power density achieved was due to the rapid thermal cycling, enabled by the thin film and microscale thermal–electrical control. The platform presented in this work could be useful to examine energy conversion in pyroelectric films at small length scales and fast time scales. The approach presented in our article could be useful for power generation in systems with rapid temperature fluctuations; for example, modern semiconductor devices such as power electronics, industrial processes such as welding and induction heating, and machines relying on fast chemical reactions such as internal combustion engines [30–32].

Funding

The authors acknowledge support from the Office of Naval Research (ONR) under Grant Number N00014-10-1-0525.

References

1. M.E. Lines and A.M. Glass. *Principles and Applications of Ferroelectrics and Related Materials*, Clarendon Press, Oxford, UK, 1977.
2. Y. Yang, W. Guo, K.C. Pradel, G. Zhu, Y. Zhou, Y. Zhang, Y. Hu, L. Lin, and Z.L. Wang, Pyroelectric Nanogenerators for Harvesting Thermoelectric Energy, *Nano Letters*, Vol. 12, pp. 2833–2838, 2012.
3. R.B. Olsen and D.D. Brown, High Efficiency Direct Conversion of Heat to Electrical Energy-Related Pyroelectric Measurements, *Ferroelectrics*, Vol. 40, pp. 17–27, 1982.
4. R.B. Olsen, D.A. Bruno, and J.M. Briscoe, Pyroelectric Conversion Cycles, *Journal of Applied Physics*, Vol. 58, pp. 4709–4716, 1985.
5. G. Sebald, S. Pruvost, and D. Guyomar, Energy Harvesting Based on Ericsson Pyroelectric Cycles in a Relaxor Ferroelectric Ceramic, *Smart Materials and Structures*, Vol. 17, p. 015012, 2008.
6. I.M. McKinley, R. Kandilian, and L. Pilon, Waste Heat Energy Harvesting Using the Olsen Cycle on 0.945Pb$(Zn_{1/3}Nb_{2/3})O_3$-0.055$PbTiO_3$ Single Crystals, *Smart Materials and Structures*, Vol. 21, p. 035015, 2012.
7. E. Fatuzzo, H. Kiess, and R. Nitsche, Theoretical Efficiency of Pyroelectric Power Converters, *Journal of Applied Physics*, Vol. 37, pp. 510–516, 1966.
8. A. van der Ziel, Solar Power Generation with the Pyroelectric Effect, *Journal of Applied Physics*, Vol. 45, pp. 4128–4128, 1974.
9. G. Cha and Y.S. Ju, Pyroelectric Energy Harvesting Using Liquid-Based Switchable Thermal Interfaces, *Sensors and Actuators A: Physical*, Vol. 189, pp. 100–107, 2013.
10. F.Y. Lee, H.R. Jo, C.S. Lynch, and L. Pilon, Pyroelectric Energy Conversion Using PLZT Ceramics and the Ferroelectric–Ergodic Relaxor Phase Transition, *Smart Materials and Structures*, Vol. 22, p. 025038, 2013.
11. A. Khodayari, S. Pruvost, G. Sebald, D. Guyomar, and S. Mohammadi, Nonlinear Pyroelectric Energy Harvesting from Relaxor Single Crystals, *IEEE Transactions on Ultrasonics Ferroelectrics and Frequency Control*, Vol. 56, pp. 693–699, 2009.
12. H.Y. Zhu, S. Pruvost, D. Guyomar, and A. Khodayari, Thermal Energy Harvesting from $Pb(Zn_{1/3}Nb_{2/3})_{0.955}Ti_{0.045}O_3$ Single Crystals Phase Transitions, *Journal of Applied Physics*, Vol. 106, p. 124102, 2009.
13. R. Kandilian, A. Navid, and L. Pilon, The Pyroelectric Energy Harvesting Capabilities of PMN-PT Near the Morphotropic Phase Boundary, *Smart Materials and Structures*, Vol. 20, p. 055020, 2011.
14. M. Ikura, Conversion of Low-Grade Heat to Electricity Using Pyroelectric Copolymer, *Ferroelectrics*, Vol. 267, pp. 403–408, 2002.
15. H. Nguyen, A. Navid, and L. Pilon, Pyroelectric Energy Converter Using Co-Polymer P(VDF-TrFE) and Olsen Cycle for Waste Heat Energy Harvesting, *Applied Thermal Engineering*, Vol. 30, pp. 2127–2137, 2010.
16. A. Navid and L. Pilon, Pyroelectric Energy Harvesting Using Olsen Cycles in Purified and Porous Poly (vinylidene fluoride-trifluoroethylene) [P(VDF-TrFE)] Thin Films, *Smart Materials and Structures*, Vol. 20, p. 025012, 2011.
17. W. Poprawski, Z. Gnutek, J. Radojewski, and R. Poprawski, Pyroelectric and Dielectric Energy Conversion—A New View of the Old Problem, *Applied Thermal Engineering*, Vol. 90, pp. 858–868, 2015.
18. B. Bhatia, A.R. Damodaran, H.N. Cho, L.W. Martin, and W.P. King, High-Frequency Thermal–Electrical Cycles for Pyroelectric Energy Conversion, *Journal of Applied Physics*, Vol. 116, p. 194509, 2014.
19. S.B. Lang, L.H. Rice, and S.A. Shaw, Pyroelectric Effect in Barium Titanate Ceramic, *Journal of Applied Physics*, Vol. 40, pp. 4335–4340, 1969.
20. D.G. Cahill, Thermal Conductivity Measurement from 30 K to 750 K—The 3ω Method, *Review of Scientific Instruments*, Vol. 61, pp. 802–808, 1990.
21. R.B. Olsen and D. Evans, Pyroelectric Energy Conversion—Hysteresis Loss and Temperature Sensitivity of a Ferroelectric Material, *Journal of Applied Physics*, Vol. 54, pp. 5941–5944, 1983.
22. B. Bhatia, J. Karthik, T. Tong, D.G. Cahill, L.W. Martin, and W.P. King, Pyroelectric Current Measurements on $PbZr_{0.2}Ti_{0.8}O_3$ Epitaxial Layers, *Journal of Applied Physics*, Vol. 112, p. 104106, 2012.
23. B.R. Holeman, Sinusoidally Modulated Heat Flow and the Pyroelectric Effect, *Infrared Physics*, Vol. 12, pp. 125–135, 1972.
24. L. Kouchachvili and M. Ikura, Improving the Efficiency of Pyroelectric Conversion, *International Journal of Energy Research*, Vol. 32, pp. 328–335, 2008.
25. F.Y. Lee, S. Goljahi, I.M. McKinley, C.S. Lynch, and L. Pilon, Pyroelectric Waste Heat Energy Harvesting Using Relaxor Ferroelectric 8/65/35 PLZT and the Olsen Cycle, *Smart Materials and Structures*, Vol. 21, p. 025021, 2012.
26. A.M. Bratkovsky and A.P. Levanyuk, Smearing of Phase Transition Due to a Surface Effect or a Bulk Inhomogeneity in Ferroelectric Nanostructures, *Physical Review Letters*, Vol. 94, p. 107601, 2005.

27. S.B. Herner, F.A. Selmi, V.V. Varadan, and V.K. Varadan, The Effect of Various Dopants on the Dielectric Properties of Barium Strontium Titanate, *Materials Letters*, Vol. 15, pp. 317–324, 1993.
28. F.D. Morrison, D.C. Sinclair, J.M.S. Skakle, and A.R. West, Novel Doping Mechanism for Very-High-Permittivity Barium Titanate Ceramics, *Journal of the American Ceramic Society*, Vol. 81, pp. 1957–1960, 1998.
29. G. Sebald, E. Lefeuvre, and D. Guyomar, Pyroelectric Energy Conversion: Optimization Principles, *IEEE Transactions on Ultrasonics Ferroelectrics and Frequency Control*, Vol. 55, pp. 538–551, 2008.
30. C.D. Rakopoulos, K.A. Antonopoulos, D.C. Rakopoulos, and E.G. Giakoumis, Investigation of the Temperature Oscillations in the Cylinder Walls of a Diesel Engine with Special Reference to the Limited Cooled Case, *International Journal of Energy Research*, Vol. 28, pp. 977–1002, 2004.
31. W.E. Newell, Transient Thermal Analysis of Solid-State Power Devices—Making a Dreaded Process Easy, *IEEE Transactions on Industry Applications*, Vol. IA-12, pp. 405–420, 1976.
32. D. Li, S.X.D. Tan, E.H. Pacheco, and M. Tirumala, Architecture-Level Thermal Characterization for Multicore Microprocessors, *IEEE Transactions on Very Large Scale Integration (VLSI) Systems*, Vol. 17, pp. 1495–1507, 2009.